Simulation of saturation transfer electron paramagnetic resonance spectra for rotational motion with restricted angular amplitude

Edmund C. Howard, Kerry M. Lindahl, Carl F. Polnaszek, and David D. Thomas

Department of Biochemistry, University of Minnesota Medical School, Minneapolis, Minnesota 55455 USA

ABSTRACT   We have simulated both conventional (V_1) and saturation transfer (V_2') electron paramagnetic resonance spectra for the case of Brownian rotational diffusion restricted in angular amplitude. Numerical solutions of the diffusion-coupled Bloch equations were obtained for an axially symmetric ^{14}N nitroxide spin label with its principal axis rotating within a Gaussian angular distribution of full width $\Delta\theta$ at half maximum. Spectra were first calculated for a macroscopically oriented system with cylindrical symmetry (e.g., a bundle of muscle fibers or a stack of membrane bilayers), with the Gaussian angular distribution centered at θ_0 with respect to the magnetic field. These spectra were then summed over θ_0 to obtain the spectrum of a randomly oriented sample (e.g., a dispersion of myofibrils or membrane vesicles). The angular amplitude $\Delta\theta$ was varied from $0°$, corresponding to no motion (order parameter = 1), to $\geq 270°$, corresponding to isotropic motion (order parameter = 0). For each value of $\Delta\theta$, the rotational correlation time, τ_r, was varied from 10^{-7} to 10^{-2} s, spanning the range from maximal to minimal saturation transfer. We provide plots that illustrate the dependence of spectral parameters on $\Delta\theta$ and τ_r. For an oriented system, the effects of changing $\Delta\theta$ and τ_r are easily distinguishable, and both parameters can be determined unambiguously by comparing simulated and experimental spectra. For a macroscopically disordered system, the simulated spectra are still quite sensitive to $\Delta\theta$, but a decrease in τ_r produces changes similar to those from an increase in $\Delta\theta$. If $\Delta\theta$ can be determined independently, then the results of the present study can be used to determine τ_r from experimental spectra. Similarly, if τ_r is known, then $\Delta\theta$ can be determined.

INTRODUCTION

Saturation transfer electron paramagnetic resonance (ST-EPR) has proven to be a powerful technique for the study of microsecond rotational motions of nitroxide spin labels (reviewed in 1–7). The most important applications of ST-EPR have been in the study of proteins in membranes, muscle filaments, and other macromolecular assemblies, in which the motions are often too slow to be detected by conventional EPR methods. Most analyses of ST-EPR spectra have depended on comparison of lineshapes with empirical reference spectra corresponding to isotropic motion, most notably spin-labeled hemoglobin in aqueous glycerol solutions (8, 9), but functionally important protein rotations are likely to be anisotropic, particularly in organized assemblies. Anisotropy of rotational diffusion has two aspects. First, the rates (diffusion constants) of rotation about different molecular axes in a rigid body may be different, due to a protein's anisotropic environment (e.g., in a membrane) or nonspherical shape, even in an isotropic environment (e.g., in solution). Second, the angular amplitudes $\Delta\theta$ of each of these modes of rotational motion is expected to be limited in most cases of motion within a protein or reorientation against an anisotropic potential (e.g., reorientation of a protein or lipid axis relative to a membrane normal).

Models that propose specific biological functions for protein rotation (e.g., in muscle contraction or transmembrane transport) usually predict restricted rotation (10, 11). Model systems for rotational diffusion with

anisotropic rates have been developed (12), but it is virtually impossible to develop reliable empirical model systems that undergo anisotropic motions with known amplitudes. Reference spectra for anisotropic motion must be obtained from theoretical simulations.

Two cases of limited-amplitude rotations are illustrated schematically in Fig. 1. Fig. 1 A shows the case with the director $\hat{n}$ parallel to the magnetic field, but θ_0 not necessarily 0. This class corresponds to motion around a preferred angle θ_0 to the director $\hat{n}$, the expected motion of myosin heads sharing a single state in a muscle fiber. Fig. 1 B shows the case with the director $\hat{n}$ not necessarily parallel to the magnetic field. This case corresponds to motion in a cone centered about the director, a commonly proposed model for the wobbling motion of lipids or proteins with respect to the membrane normal (13).

We simulated the spectra of disordered systems as a sum of spectra of distributions over θ_0. This corresponds approximately to the data expected for a randomly oriented sample, such as a dispersion of membranes or myofibrils, although rigorous simulation would require the explicit variation of ψ, the angle between the director $\hat{n}$ (membrane normal or fiber axis) and the magnetic field (14), increasing computing time by an order of magnitude. The approximation used for randomly oriented samples in the present study is more rigorous than that of Mason et al. (15), which has been used to simulate spectra from random lipid dispersions (16, 17).

None of Harden McConnell's many contributions to the theory of magnetic resonance has been more profound and far-reaching than his insight into the spectral effects of molecular dynamics. Two direct ancestors of
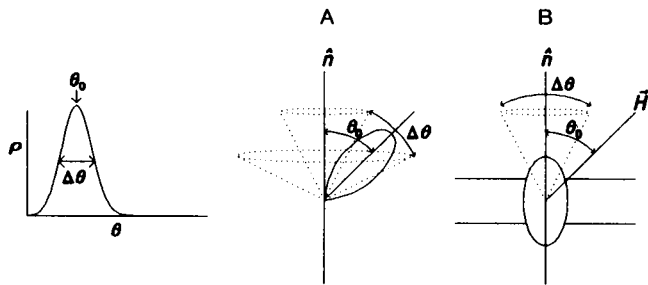
FIGURE 1 Motional models for restricted diffusion in an angular band of full width $\Delta\theta$, centered at θ_0, as illustrated by the orientational distribution at left. (A) Model with the director $\hat{n}$ (e.g., a muscle fiber axis) parallel to the Zeeman field but at an angle θ_0 to the preferred probe orientation. (B) Model with the director $\hat{n}$ (e.g., a membrane normal) parallel to the preferred probe orientation but at an angle θ_0 to the Zeeman field.

the present study are McConnell's modification of the Bloch equations to include the effects of chemical exchange between two magnetically different environments (18) and his application of this idea to the calculation of conventional EPR spectra corresponding to isotropic rotational diffusion (19). Thomas and McConnell (20) extended these diffusion-coupled Bloch equations to the simulation of ST-EPR spectra, and model-system experiments (9) verified the accuracy of this class of simulations, which have been performed by numerical solution of either diffusion-coupled Bloch equations (9, 20) or mathematically equivalent density matrix equations (4, 21). Simulations corresponding to anisotropic rotations have been reported by Robinson and Dalton (22, 23), but those studies dealt only with motions corresponding to the free rotation of a rigid body that could have different diffusion constants about different molecular axes but not restricted motion amplitudes. Furthermore, to minimize computing time, most of those theoretical studies on anisotropic motion dealt mainly with dispersion (U'_1) spectra of ^{15}N-nitroxide spin labels (22), with only a few examples given for the absorption (V'_2) case (23), despite the fact that virtually all biological applications of ST-EPR have been V'_2 experiments on ^{14}N-nitroxide spin labels (4, 6, 7). In the present study we report the simulation of absorption ST-EPR (V'_2) spectra of ^{14}N-nitroxide spin labels undergoing rotational motions restricted in angular amplitude for samples with cylindrical symmetry and samples with complete macroscopic disorder.

METHODS

The methods used in the present study are an extension of those given previously for transition-rate calculations for isotropic motion (19, 20). The expressions for the magnetization couplings due to spin relaxation (including the relaxation times, T_1 and T_2, and the amplitude of the applied microwave field, H_1), modulation effects (sensitive to the modulation amplitude, H_m, and the modulation frequency, v_m) and resonant frequencies (which depend on the g and T tensors and the

orientation of their components in the Zeeman field) can be found in the above two references.

Only the motion part of the set of coupled equations needs to be modified for restricted diffusion. As in the previous transition-rate studies, we allow transitions only between adjacent equally spaced angular zones, thus simulating Brownian diffusion; when the magnetic tensors are axially symmetric, as assumed here, only a grid of zones with respect to the polar angle θ (the angle between the nitroxide principal axis and the field) is required. A population distribution (14, 53) with Gaussian polar angular distribution centered at θ_0 and of full width at half maximum $\Delta\theta$ has the form

$$\rho(\theta) = \exp\left(-4 \log 2\left(\frac{(\theta - \theta_0)}{\Delta\theta}\right)^2\right). \tag{1}$$

Isotropic motion is simulated by making $\Delta\theta$ large enough that an increase causes no change in the spectrum. We have found 270° sufficient. Spectra for single distributions were normalized by the integral of ρ.

We simulated Brownian diffusion within each distribution on a grid of N angular zones, with N determined by the evaluation range (here $2.8\Delta\theta$) and N_{90}, the number of angular zones in 90°. The probability of a transition from the ith angular zone to an adjacent zone is given by (24):

$$\Pi(\theta_i, \theta_{i+1}) + \Pi(\theta_i, \theta_{i-1}) = \frac{N_{90}^2}{3\pi^2\tau_r} = \frac{2N_{90}^2 D}{\pi^2}$$

$$\Pi(\theta_i, \theta_{i\pm1})n_i = \Pi(\theta_{i\pm1}, \theta_i)n_{i\pm1}, \tag{2}$$

with

$$n_i = \int_{\theta_i-\delta/2}^{\theta_i+\delta/2} \rho(\theta) \sin\theta \, d\theta$$

and

$$\delta = \theta_i - \theta_{i-1} = \pi/2N_{90}.$$

D is the rotational diffusion coefficient. In the present study, we define the rotational correlation time τ_r to be $1/(6D)$ and will use this convention in the presentation and discussion of our results. The rigorous definition of a correlation time in this case, the exponential decay constant for $\langle P_2(\cos\theta)\rangle$ for the case of axial tensors, would be a complex function of D and $\Delta\theta$ and would be $1/(6D)$ only for isotropic motion (6, 25–28).

With these modifications to the transition-rate formalism, conventional and ST spectra can be calculated for systems in which there is a Gaussian orientation distribution of molecules of full width at half maximum $\Delta\theta$ about θ_0. To calculate the spectra resulting from a random distribution of orientations, the spectra calculated at each value of θ_0 must be summed over a sufficiently fine grid of distributions.

The formalism presented above was incorporated into a system of linear equations (20) that are a function of the magnetic tensors, relaxation times, both microwave and modulation frequencies and amplitudes, harmonics of the modulation frequency (both in-phase and in-quadrature), the rotation rate, and the band angle. The range of angular zones included in each calculation was sufficiently broad ($2.8\Delta\theta$) that an increase caused no significant effect on the simulated spectrum. Other truncation parameters, such as the number of angular zones in 90° (N_{90}) and the number of modulation harmonics included, were also varied to ensure convergence. This system of linear equations (e.g., $\sim$1,250 equations for $\Delta\theta = 30°$) was solved for the magnetization components (V_1, V'_2, etc.). For an oriented sample (only one value of θ_0), the system of equations must be solved separately three times (once for each value of the nitrogen nuclear spin) for each value of the magnetic field H. To simulate the spectrum of a randomly oriented sample, this calculation was repeated for a mesh of θ_0 values from 0 to

Hyperfine tensor	
$T_\parallel$	35 G
$T_\perp$	7 G
g Tensor	
$g_\parallel$	2.00241
$g_\perp$	2.00741
Relaxation times	
T_1	6.6×10^{-6} s
T_2	2.4×10^{-8} s*
Field values	
Range	100 G
Center of spectrum	3,400 G
Mesh	0.5 G

Microwave and modulation amplitudes

	H_1	H_m	Number of harmonics
	G	G	
V_1	0.01	0.01	0
V_2'	0.25	5.0	4

* This corresponds to a rotationally invariant linewidth $2/(\sqrt{3}\,|\gamma|\,T_2)$ of 2.7275 G peak-to-peak (50).

90°. Most of the calculations were performed on a Cray-2 (Cray Research, Inc., Eagan, MN) computer using Cray SCILIB banded linear equation routines.

A typical calculation used the parameters in Table 1 with θ_0, $\Delta\theta$, and τ_r as variable inputs. Simulating a single spectrum for a random distribution (e.g., Fig. 4) required four harmonics, 40 values of θ_0, and 12–112 angular zones (N_{90}). Such simulations, when calculated for 201 field positions, took from 9 to 98 processor minutes on a Cray-2. The spectral parameters L''/L, C'/C, and H''/H generated with 40 values of θ_0 and $N_{90} = 40$ were within 1% of the values obtained with 60 values of θ_0 and $N_{90} = 60$ for the worst case (data not shown). Spectra for unrestricted motion were simulated with $\Delta\theta = 270°$; spectra for $\Delta\theta = 0°$ were simulated with $\Delta\theta = 1°$ and $N_{90} = 180$.

RESULTS

We examine first the effect of changing $\Delta\theta$ on both conventional and ST-EPR spectra, with τ_r fixed at 10^{-7} s. The other parameters used in all the simulations are given in Table 1. This correlation time is near the rigid limit for V_1 spectra (i.e., there is very little effect on the spectrum even for unrestricted [isotropic] motion), since $\tau_r > T_2 \approx 2.4 \times 10^{-8}$ s, the spin–spin relaxation time used in our simulation (Table 1). This value of T_2 has been established from previous simulations on isotropic systems for V_1 spectra (19, 29). In contrast, this value of τ_r is near the rapid limit for V_2' spectra (provides maximal ST effects), since $\tau_r < T_1 \approx 6.6 \times 10^{-6}$ s, the spin–lattice relaxation time (6, 7). The parameters used to characterize ST-EPR spectra, line height ratios (6–9), and ratios of spectral integrals (8, 30) are not very sensitive to changes in τ_r near this τ_r. The rigid limit for V_2' is reached when $\tau_r \gg T_1$, as established from previous simulations on isotropic systems for V_2' spectra (9, 20). We

used $\tau_r = 10^{-2}$ s to calculate the ST-EPR rigid-limit spectra; these spectra were virtually indistinguishable from those for $\tau_r = 10^{-3}$ s.

Oriented sample: vary $\Delta\theta$

Fig. 2 shows the effect on the spectrum of varying $\Delta\theta$ with θ_0 fixed at 0°. The columns of Fig. 2 are, from left to right, V_1 spectra at $\tau_r = 10^{-7}$ s, V_2' spectra at $\tau_r = 10^{-7}$ s, and V_2' spectra at $\tau_r = 10^{-2}$ s. The V_1 spectra in Fig. 2 are nearly identical to those for $\tau_r = 10^{-2}$ s (not shown), so V_1 spectra are determined almost exclusively by orientation in this time range. V_2' spectra show both orientation and motion sensitivity. Comparison of the V_2' spectra in the central and right columns show that at $\theta_0 = 0°$, there is little motion sensitivity for highly ordered systems (those with $\Delta\theta < 30°$) and that sensitivity to motion increases as the order decreases.

Oriented sample: vary θ_0

Fig. 3 shows the effect on the spectrum of varying θ_0 with $\Delta\theta$ fixed at 30°. The columns are as in Fig. 2. These results are applicable to the muscle fiber schematically illustrated in Fig. 1 A. θ_0 is known for muscle from several species (14, 31). The simulations in Fig. 3 show that V_2' spectra for oriented systems will be most sensitive to restricted motion when θ_0 is near 45°.

Random distributions of the director: sum over θ_0

Fig. 4 shows V_1 and V_2' spectra that would result from limited-amplitude reorientation of the nitroxide principal axis in randomly oriented systems. Most ST-EPR and conventional EPR experiments are carried out on such systems (e.g., lipid or membrane dispersions, protein solutions, or myofibril dispersions) in which there is no preferred orientation of the director (membrane normal or fiber axis) relative to the applied field. The spectra corresponding to the V_2' rigid limit (the right columns of Figs. 2 and 3) are omitted from this figure, since, for random distributions, the rigid limit spectra do not vary with $\Delta\theta$ and are identical to the $\Delta\theta = 0°$ spectrum (Fig. 4, top right). The effects of restricted motion are almost negligible in the V_1 spectra (Fig. 4, left), since the correlation time is near the rigid limit, although there is still some motional narrowing. V_2' spectra (Fig. 4, right) vary considerably with $\Delta\theta$.

In these randomly oriented systems, in contrast to oriented ones (Figs. 2 and 3), the effects of restricted motion are similar to those of increased correlation time. This may be seen in Fig. 5, which shows the combined effect of changes in $\Delta\theta$ and τ_r. Spectra for $\tau_r = 10^{-2}$ s are omitted; spectra for the rigid limit are identical to spectra with $\Delta\theta = 0$.

Fig. 6 shows the line-height ratios commonly used to parameterize V_2' spectra (8, 9) plotted as a function of $\Delta\theta$ for various values of τ_r. The low-field parameter $L''/$
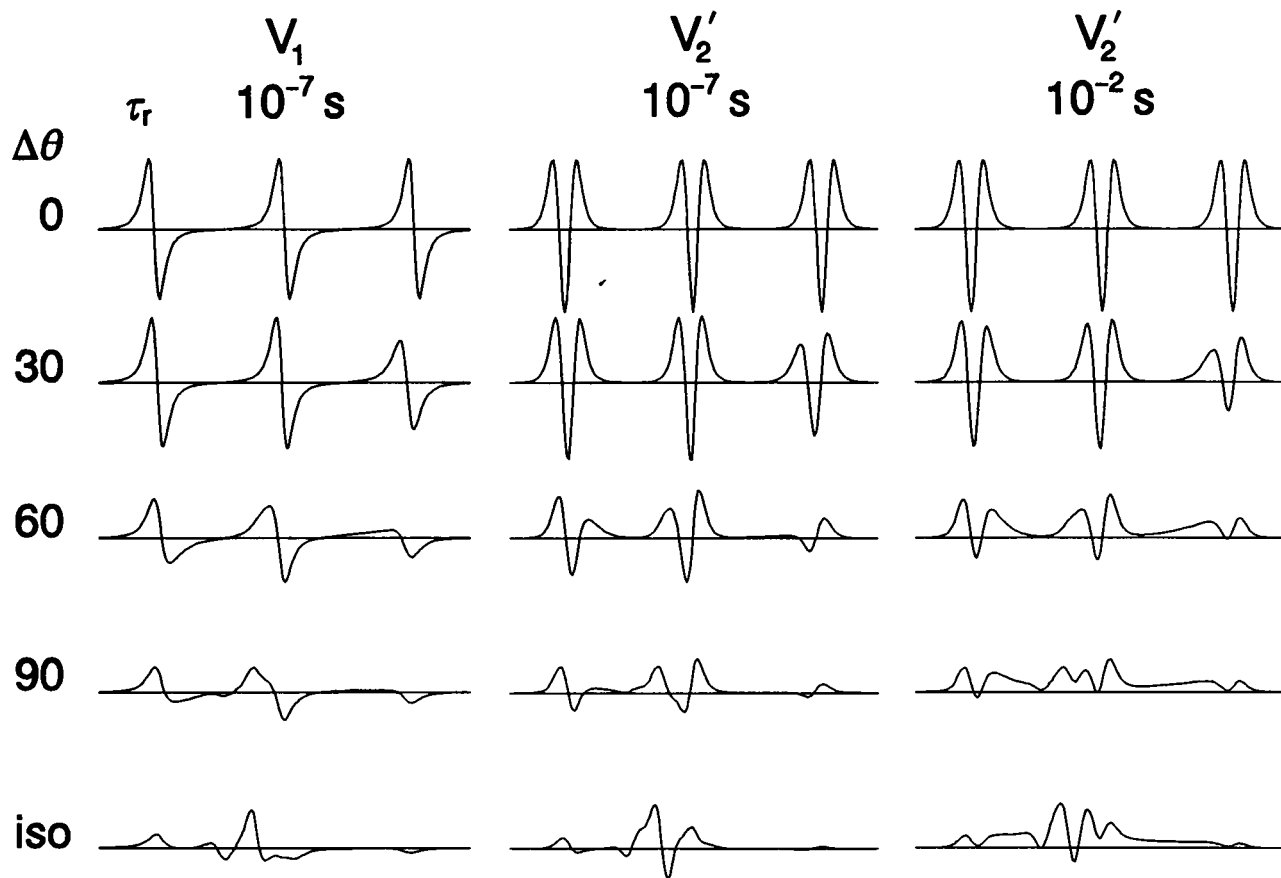
FIGURE 2 Simulated conventional (V_1) and ST (V'_2) EPR spectra for Gaussian restricted rotational motion of full width $\Delta\theta$ in an oriented sample with θ_0 (the preferred tilt angle) fixed at $0°$. *Left,* V_1 spectra for a correlation time ($\tau_r = 1/6D$) of 10^{-7} s, near the rigid limit, where motional effects are negligible. *Center,* V'_2 spectra, also for $\tau_r = 10^{-7}$ s, near the rapid limit, where motional effects from ST are maximal. *Right,* V'_2 spectra for $\tau_r = 10^{-2}$ s, near the rigid limit, where motional effects from saturation transfer are negligible. All V_1 spectra are to the same scale, as are all V'_2 spectra.

L appears to be sensitive to the largest range of $\Delta\theta$ values, and the high-field parameter H''/H is most sensitive to smaller amplitude motions. In all three plots, the ratio decreases to a limiting value for each correlation time, and that value is lower for shorter correlation times. For each value of τ_r, there appears to be a $\Delta\theta_{max}$, above which there is no further effect of motion on the spectrum, and $\Delta\theta_{max}$ increases as τ_r decreases. We show in Discussion that this result is easily explained by the principles of saturation transfer.

These V'_2 spectral ratios usually have been used to estimate correlation times from experimental spectra, using plots of the ratios against τ_r for isotropic motion (2, 8, 9). Since these parameters can also be affected by $\Delta\theta$ (Fig. 6), with the value of the parameters varying over the same range as in the case of isotropic motion, it is clear that no single parameter can be used to determine unambiguously the actual τ_r independently of $\Delta\theta$. We define the effective correlation time τ_r^{eff} to be the τ_r that would be estimated from a given spectral parameter, using a plot of that parameter versus τ_r for isotropic rotational motion (8, 9). τ_r^{eff} is equal to τ_r only for the bottom row (isotropic motion) of Fig. 7, is usually greater

than τ_r when motion is restricted, and is undefined ($>10^{-3}$ s for V'_2 spectra) for $\Delta\theta = 0°$ (Fig. 4, *top row*). The determination of effective correlation times from a V'_2 spectrum resulting from restricted motion is illustrated in Fig. 8, which shows the V'_2 spectra for isotropic motion that have the same values of the ratio parameters as those obtained from our restricted motion simulation with $\Delta\theta = 30°$ and $\tau_r = 10^{-7}$ s. The three effective correlation times are all greater than the actual correlation time, as expected, but they are also significantly different from each other. That is, although the overall lineshapes for restricted motion are similar to those for isotropic motion, there is no isotropic-motion spectrum that matches the restricted-motion spectrum precisely. The lineshape itself provides enough information to conclude that the motion is not isotropic. In fact, other spectral features are even more sensitive to the deviation from isotropic motion, notably the relative amplitudes of the two peaks to the right of peak C (C'' and H^* in Fig. 6). The effective correlation times obtained from the ST-EPR amplitude parameters for isotropic rotational motion are plotted against $\Delta\theta$ in Fig. 9. The calibration curves for isotropic rotation were simulated using the
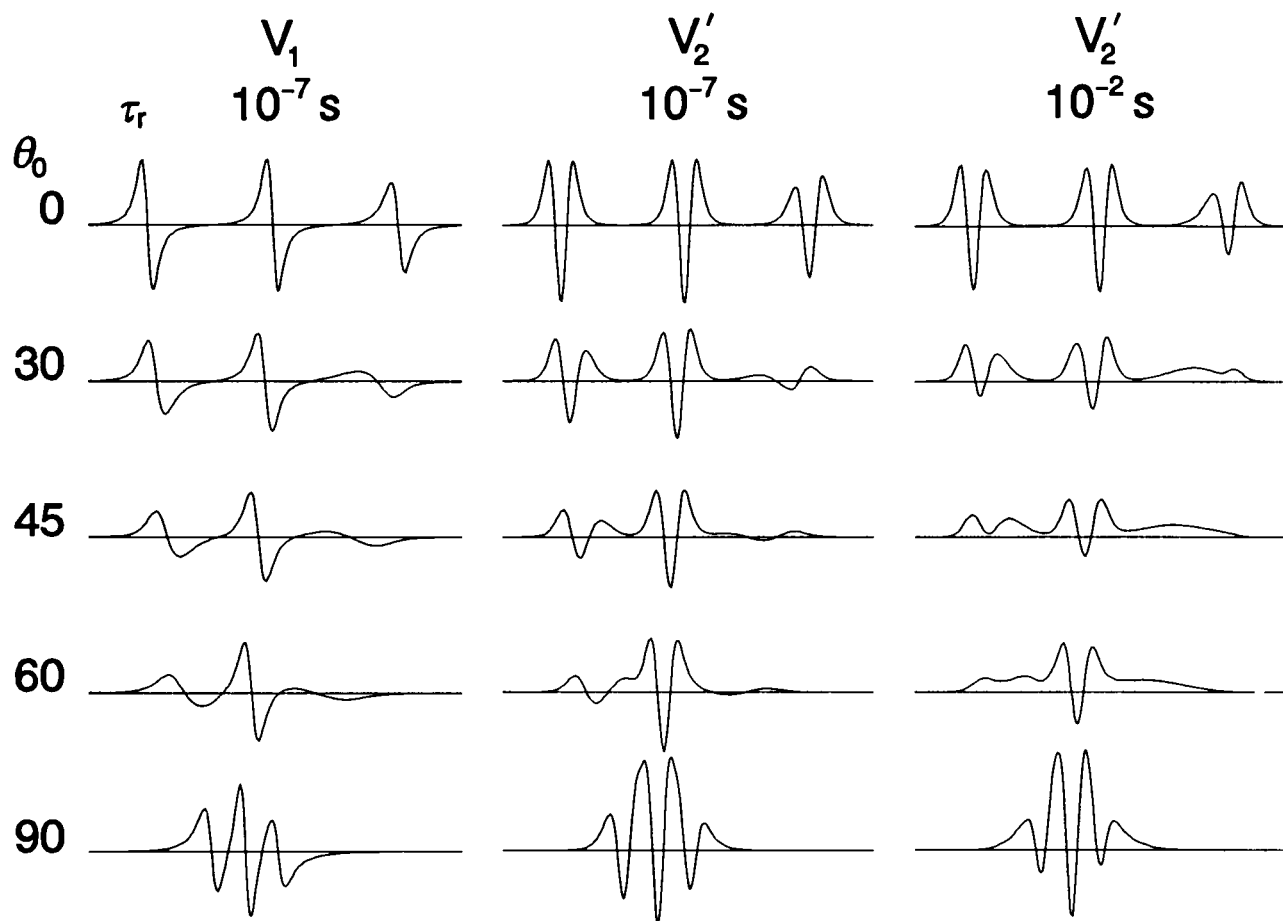
FIGURE 3 Conventional and ST-EPR spectra simulated for Gaussian wobble with a full-width $\Delta\theta$ of 30° as a function of the angle θ_0 between the center of the distribution and the magnetic field. *Left,* V_1 spectra at $\tau_r = 10^{-7}$ s. *Center,* V'_2 spectra at $\tau_r = 10^{-7}$ s. *Right,* V'_2 spectra at $\tau_r = 10^{-2}$ s. All V_1 spectra are to the same scale, as are all V'_2 spectra.

same parameters as our restricted motion calculations. The effective correlation times obtained from the L''/L and H''/H parameters are much greater than the actual τ_r.

Another parameter used to analyze ST-EPR spectra is $\int V'_2$, the integral of the V'_2 spectrum normalized by the double integral of the V_1 spectrum at low H_1 and low H_m (30). This parameter is sensitive not only to lineshape changes but also to the decrease in overall spectral intensity as ST (motion) increases. For isotropic motion, this integral parameter is sensitive to τ_r in the same region as the lineshape parameters (30). For restricted-amplitude motion, the integral parameter shows intermediate sensitivity between the low-field parameter L''/L and the high field parameter H''/H, as shown by the effective correlation times plotted in Fig. 9.

DISCUSSION

Summary of results

The simulations in Figs. 2–7 show that V'_2 ST-EPR spectra are sensitive to the amplitude $\Delta\theta$ as well as the rate D

$(1/6\tau_r)$ of rotational motion. For macroscopically oriented samples (Figs. 2 and 3), amplitude and rate effects are clearly distinguishable, and the additional parameter θ_0 can be extracted as long as the amplitude is small. Thus, spectra like those in Figs. 2 and 3 can be used to determine all three parameters (θ_0, $\Delta\theta$, and τ_r) from an experimental spectrum. For randomly oriented samples (a more common experimental condition), the spectral analysis is more ambiguous: a reduction in the amplitude of motion (smaller $\Delta\theta$) results in a spectrum that is similar to that resulting from slower rotational motion (greater τ_r) at the same $\Delta\theta$. However, the spectral parameters used to characterize correlation times for isotropically rotating systems give different effective correlation times when applied to a single spectrum resulting from limited-amplitude motion (Figs. 8 and 9), implying that the lineshapes are, in principle, distinguishable from those corresponding to isotropic motion.

Interpretation

The dependence of spectral parameters on $\Delta\theta$ and τ_r (Figs. 6 and 7) provides insight into the mechanism of saturation transfer by rotational diffusion. In Fig. 6, each
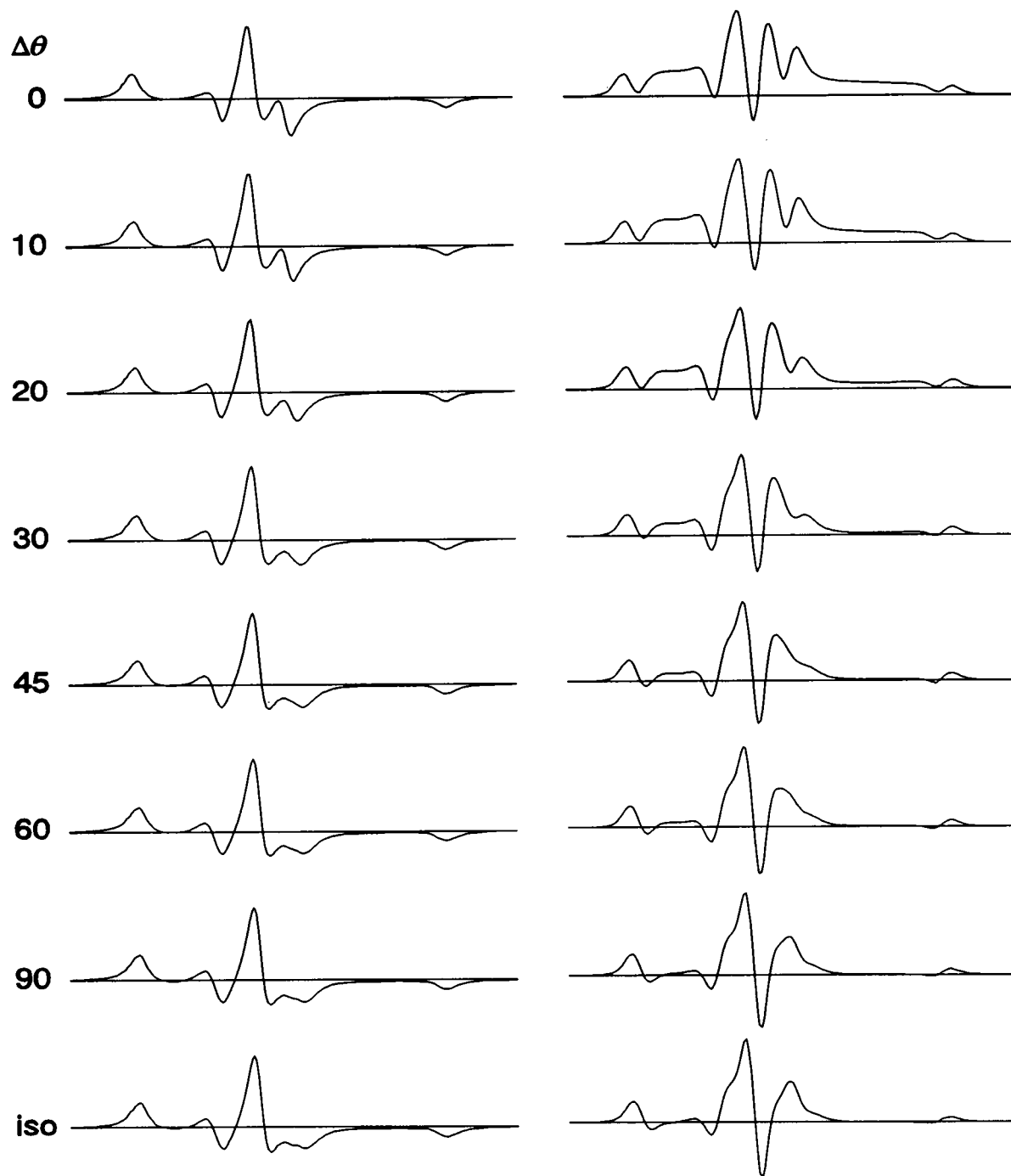
$\Delta\theta$

0

10

20

30

45

60

90

iso

FIGURE 4 Theoretical conventional and ST spectra for an isotropic (random) distribution of orientations θ_0 at different full widths $\Delta\theta$. *Left*, V_1 spectra at $\tau_r = 10^{-7}$ s (near rigid limit). *Right*, V'_2 spectra at $\tau_r = 10^{-7}$ s (rapid limit). The spectra were simulated by summing individual spectra at 40 values of θ_0. All spectra in a column are to the same scale.

of the three parameters decreases to a constant limiting value as $\Delta\theta$ increases. Since an increase in either the rate or amplitude of motion causes a decrease in each of these line height ratio parameters, the limiting value is lower for shorter correlation times τ_r. For each value of τ_r, there appears to be a $\Delta\theta_{max}$ above which there is no further effect on the spectrum (Fig. 6); i.e., $\tau_r^{eff} = \tau_r$ for $\Delta\theta \geq$

$\Delta\theta_{max}$ (Fig. 9). Note that $\Delta\theta_{max}$ decreases as τ_r increases. For example, at $\tau_r = 10^{-6}$ s, L''/L is sensitive to changes in $\Delta\theta$ up to $\Delta\theta_{max} = 90°$, but at $\tau_r = 10^{-4}$ s, there is virtually no change beyond $\Delta\theta_{max} = 10$–$20°$ (Figs. 6 and 9). This can be rationalized by the following argument (7). Saturation transfer can be caused only by rotational motion that occurs within the excited-state lifetime (lon-
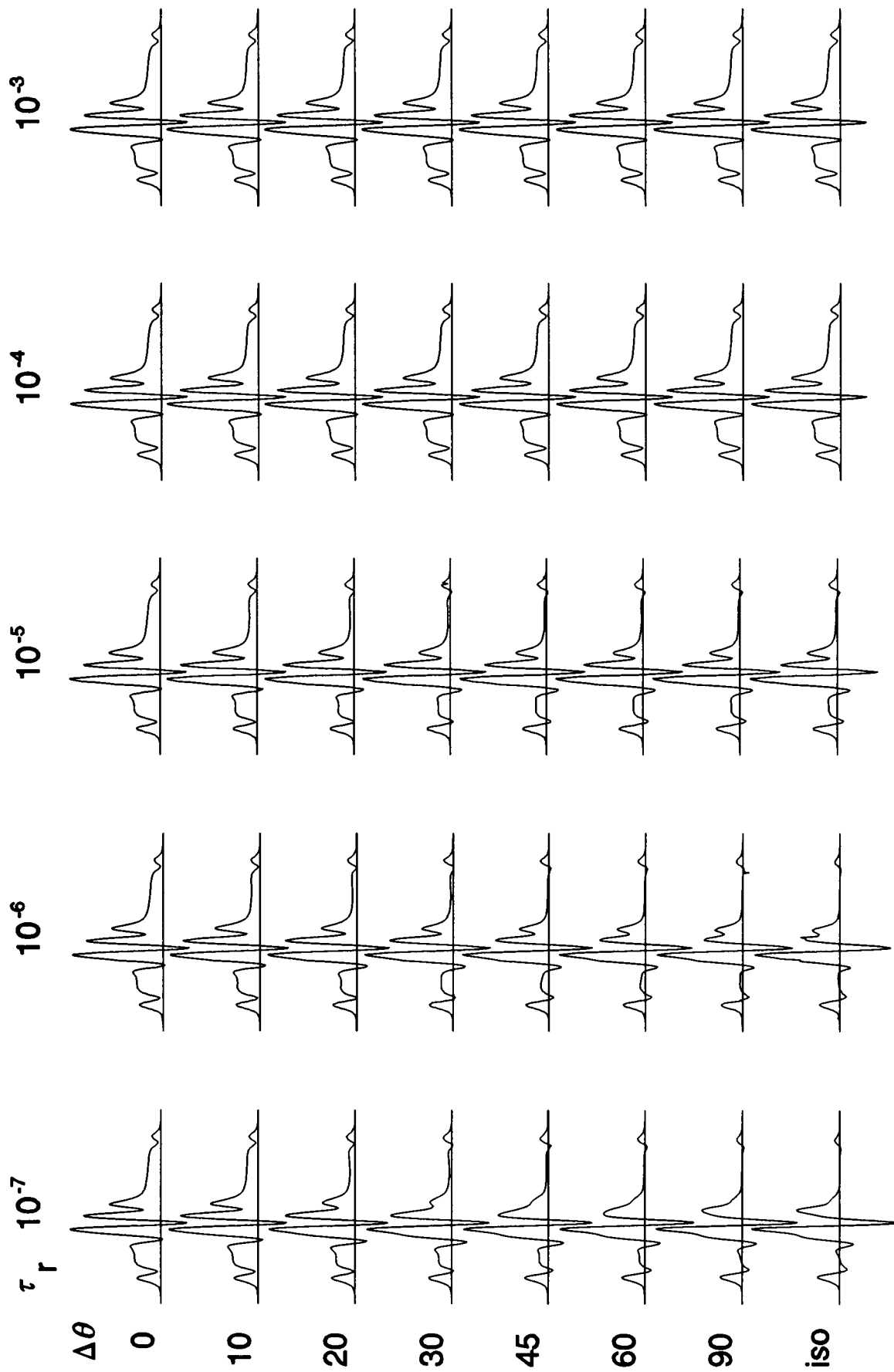
FIGURE 5 Simulated V_2' spectra for an isotropic distribution of orientations θ_0 at correlation times τ_r from 10^{-7} to 10^{-3} s and amplitudes $\Delta\theta$ from 0 to isotropy. All spectra are to the same scale.

FIGURE 7 Variation of the line height ratios with the correlation time τ_r for various values of $\Delta\theta$: (A) H''/H, (B) C'/C, (C) L''/L.
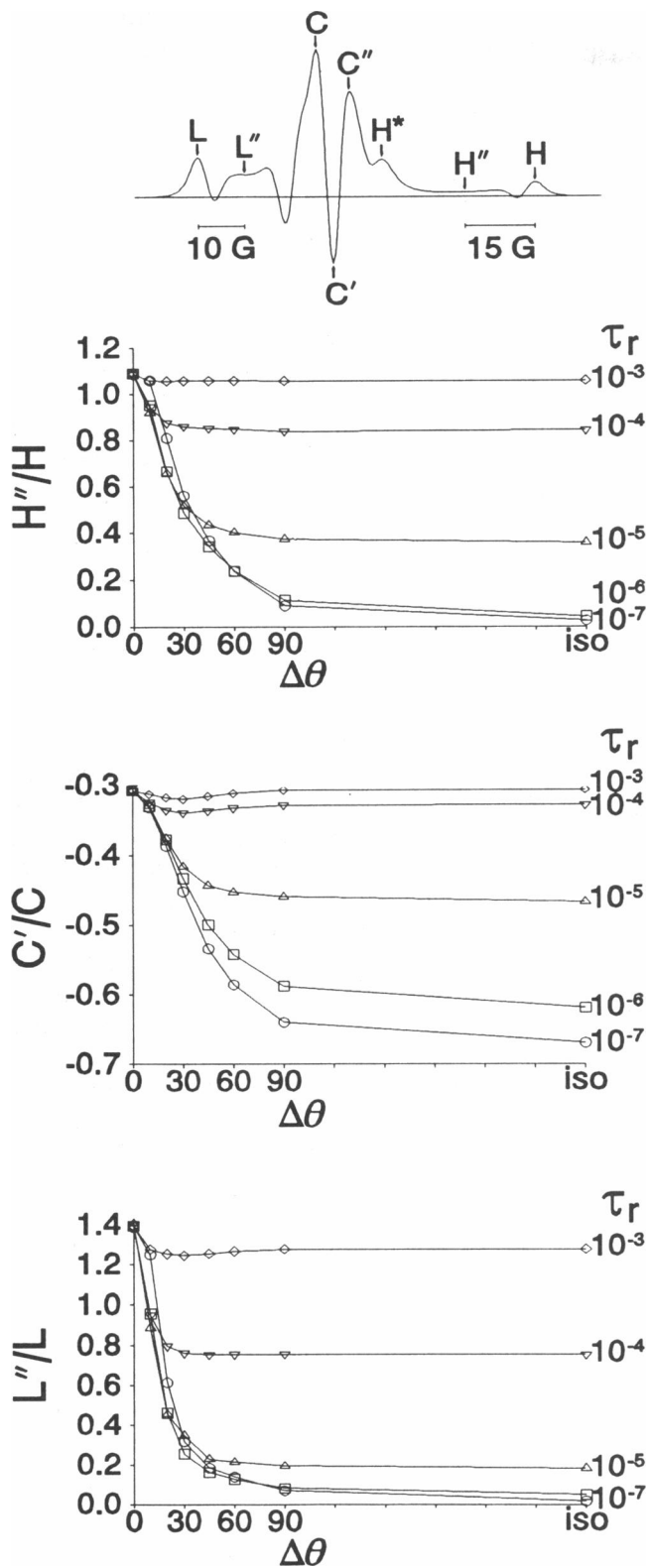

FIGURE 6 Variation of the line height ratios as a function of the distribution full width $\Delta\theta$ at various correlation times. The spectrum at the top shows how the line heights are defined. The line height L'' is defined to be 10 G above the low field extremum L, and the line height H'' is defined to be 15 G below the high field extremum H (corresponding to $\theta = 45°$) (8). These conventions are slightly different than those used by others (9, 42).

gitudinal relaxation time, $T_1 \approx 10^{-5}$ s) of a spin label. The r.m.s. angle of rotation within a time t is $0.5\Delta\theta_{rms} = 2t/3\tau_r$ (7). Therefore, the largest amplitude rotation that can have an effect on saturation transfer is the lesser of 90° and $\Delta\theta_{max} \approx 4T_1/3\tau_r$, which is 760° for $\tau_r = 10^{-6}$ s and 8° for $\tau_r = 10^{-4}$ s, in good agreement with the $\Delta\theta_{max}$ values of Fig. 6. For long τ_r values ($\geq 10^{-4}$ s) and/or large $\Delta\theta$ values, the ST-EPR spectrum is insensitive to changes in $\Delta\theta$; i.e., $\tau_r^{eff} = \tau_r$ (Fig. 9).

FIGURE 8 Comparison of a V'_2 spectrum simulated for a random distribution of θ_0 at $\tau_r = 10^{-7}$ s and $\Delta\theta = 30$ degrees with isotropic (unrestricted motion) spectra giving the same line height ratios. E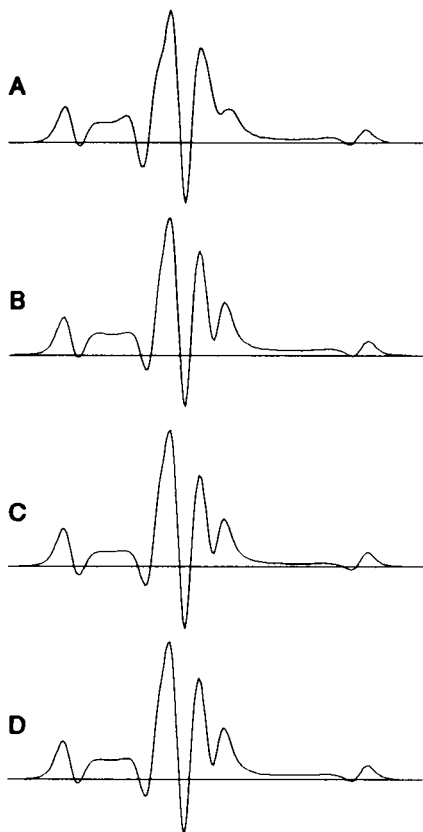ffective correlation times were determined using the plots in Fig. 7, and the corresponding spectra are shown here. (*A*) Restricted motion. (*B*) Isotropic motion at $\tau_r = 2.840 \times 10^{-5}$ s, with L''/L matching *A*. (*C*) Isotropic motion with a correlation time of 1.174×10^{-5} s, with C'/C matching *A*. (*D*) Isotropic motion with a correlation time of 2.195×10^{-5} s, with H''/H matching *A*. All spectra are to the same scale.

Relationship to previous experimental work

In this section we will comment briefly on the relationship of these simulations to ST-EPR spectra of biomolecules. We do not intend to carry out here any detailed analysis of published spectra but rather to point out some potential applications. We consider mainly applications to membranes and muscle fibers, since these systems can be studied either in a macroscopically oriented sample (Figs. 2 and 3) or a randomly oriented dispersion (Figs. 4–9). The motions that are expected to be slow enough for ST-EPR studies include those of large proteins, especially in assemblies, and those of lipids that are either in the gel phase or interacting strongly with proteins.

Our simulations of spectra corresponding to oriented samples (Figs. 2 and 3) are applicable to the analysis of experiments performed on fatty acid and phospholipid spin probes and spin-labeled membrane proteins with the nitroxide principal axis parallel to the membrane

normal (see Fig. 1 *B*) and the membrane normal parallel to the field. This is a commonly achieved experimental condition for lipid probes having the doxyl group. Delmelle et al. (32) recorded V'_2 spectra of the spin label 5-doxyl stearic acid in oriented films of dipalmitoyl phosphatidyl choline-cholesterol in the gel phase and found that the ratio C'/C varied markedly with temperature. For such highly ordered systems ($\Delta\theta \le 20°$), C'/C does not change much with $\Delta\theta$ or with τ_r (Figs. 6 and 7). Thus, the variation of C'/C seen by Delmelle et al. was probably not due to a change in the amplitude of lipid chain wobble but rather to a change in the rate of rotation about the membrane normal. The spectra shown in Fig. 3 indicate that the maximal sensitivity to motion in a highly ordered system ($\Delta\theta = 30°$) occurs at angles θ_0 in the range of 30–60°. This suggests that spectra taken at these orientations will yield information primarily about motion, whereas spectra taken at the more typical parallel and perpendicular orientations will yield information primarily about orientation distribution. ST-EPR spectra obtained on oriented bilayers at variable values of θ_0 are consistent with this principle (33).

Another oriented system is spin-labeled myosin in the helical arrays of muscle fibers (34). This system is particularly relevant to the present simulations, since restricted-amplitude motions have been predicted to be crucial to myosin's role in force generation (11) and nonrandom orientation distributions of myosin heads have been detected by EPR and other methods (14, 34). Comparison of spectra like those in Fig. 2 with those obtained in muscle fibers (35) indicates that actin-bound myosin heads have very little disorder ($\Delta\theta \approx 15°$) and have no submillisecond rotational motion ($\tau_r \ge 10^{-3}$ s).

The most common experimental situation is that of a random distribution of ordered assemblies, correspond-
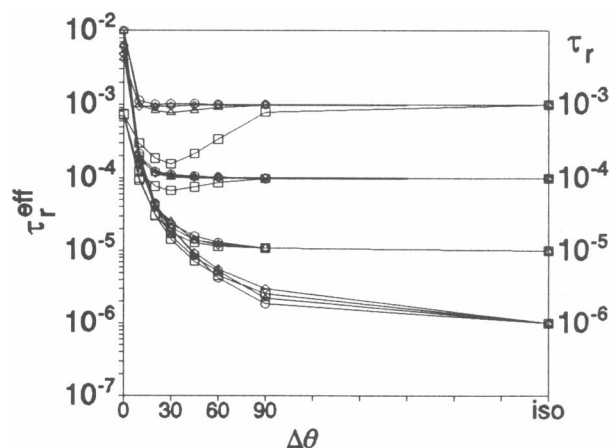

FIGURE 9 Effective isotropic correlation times of restricted motion spectra, calculated from the line height ratios and normalized V'_2 integral for isotropic rotational diffusion, plotted for correlation times τ_r of 10^{-3}, 10^{-4}, 10^{-5}, and 10^{-6} s. ○, from L''/L; □, from C'/C; △, from H''/H; ◇, from $\int V'_2$.

ing to Figs. 4–9. For such systems, the effective correlation times have been measured using the calibration curves for isotropic rotational motion (8, 9). Fig. 9 shows that a restricted rotational amplitude can yield a τ_r^{eff} that is substantially longer than τ_r. If the τ_r can be determined independently, then Fig. 9 can be used to determine $\Delta\theta$. For example, the effective correlation time obtained for spin-labeled myosin filaments (from L''/L) is $\tau_r^{\text{eff}} = 13$ μs (34), but the best estimate for the actual correlation time, obtained from time-resolved phosphorescence, is $\tau_r = 3.3$ μs (36). Using a plot of τ_r^{eff} versus $\Delta\theta$ (made as in Fig. 9, from a plot of L''/L vs. $\Delta\theta$, except with τ_r fixed at 3.3 μs), we obtain $\Delta\theta = 40°$. In other cases, independent information about $\Delta\theta$ can be used to determine the actual τ_r. For example, the effective correlation time obtained for spin-labeled actin filaments, assuming isotropic motion, using only the parameter L''/L, was $\tau_r^{\text{eff}} = 52$ μs (37). In a subsequent study on flow-oriented actin, $\Delta\theta$ was determined to be 53° (38). Fig. 9 shows that for this combination of a long τ_r^{eff} and a large $\Delta\theta$, $\tau_r = \tau_r^{\text{eff}}$.

Even for these randomly oriented samples, our calculations show that the effective correlation time often depends on the spectral parameter measured (Fig. 9); i.e., the V_2' spectrum for restricted amplitude motion does not necessarily match any of the spectra corresponding to isotropic motion (Fig. 8). The main discrepancies are observed when comparing C'/C with other parameters. Examples of this have been reported for muscle proteins in solution (39), muscle fibers (34), membrane proteins (40), viral proteins (41), and lipid probes (32, 33, 42, 43). Various kinds of anisotropic motion have been ascribed to this type of observation. It frequently has been suggested that the deviation from isotropy corresponds to preferential (unrestricted) motion about a particular molecular axis (59) (e.g., the membrane normal), however, Figs. 6–9 show that restricted amplitude motion also can give rise to this phenomenon in ST-EPR spectra. In summary, our limited-amplitude motion model with a single correlation time predicts many of the features observed experimentally for systems likely to undergo restricted motion, despite the common tendency to ascribe these features to axial motion.

Relationship to other theoretical work

Based on the above discussion, it is clearly of interest to compare the effects of restricted amplitude motion (present study) with those of the case of unrestricted motion with different rates about the principal axis ($D_\parallel$) and the axes perpendicular to the principal axis ($D_\perp$) (22, 23, 60, 61). For those cases in references 4, 22, and 23 with ($D_\parallel/D_\perp$) large and for purely axial motion ($D_\perp = 0$), the ST-EPR line-shape parameters show similar effects to those observed in the present study: spectra do not match those corresponding to isotropic motion. Gaffney (12) observed this effect experimentally. It seems likely that the effects of these two different types of anisotropic motion (restricted amplitude versus uniaxial rotation) should be distinguishable. However, to see whether this ambiguity can be resolved in a practical way, a quantitative comparison of the effects of the two models will require the simulation of spectra corresponding to both models with the same mathematical formalism, nitrogen isotope, and other assumptions. These studies are underway.

Theoretical studies that include restricted amplitude motion have been carried out for both conventional (V_1) EPR and for optical anisotropy. In both fields, the motion model usually has been a restricted random walk within a rigid cone, in contrast to the more physically realistic Gaussian distribution considered in the present study, but it has been shown that the essential results are model-independent and are applicable to any restricted-amplitude rotational motion (26, 27). Early simulations were restricted to the rapid-motion limit. That is, the rate of rotation within $\Delta\theta$ was assumed to be rapid enough ($\tau_r < 10^{-10}$ s for both conventional EPR and fluorescence) that an increase in rate (decrease in τ_r) would cause no further effect on the V_1 EPR spectrum (44, 45, 62) or the steady-state optical anisotropy (46). Under these conditions, the spectrum can be characterized by a single parameter $\Delta\theta$ (or, equivalently, by the order parameter S, which decreases with $\Delta\theta$). A more general model, in which correlation times can be intermediate between the rapid and static limits (10^{-10}–10^{-7} s for both conventional EPR and fluorescence) and data are thus sensitive to both the amplitude and rate, has been analyzed for optical anisotropy experiments (25, 47, 48) and nuclear magnetic resonance relaxation experiments (27, 48).

An equivalent approach, using diffusion in a restricted potential, has been applied to conventional EPR (49, 50). That technique, involving an eigenfunction expansion and the density-matrix formalism (4), is less efficient than the transition-rate method in simulating ST-EPR spectra for restricted slow motion. Robinson et al. (51) have developed a versatile technique for simulating EPR spectra from molecular trajectories. This approach has not yet been extended to ST-EPR but provides a straightforward method of simulating restricted-motion spectra, although it will be significantly slower than the transition-rate method if the time needed to simulate V_1 spectra of isotropic systems is a reliable guide (51). The transition-rate method has been applied successfully to the simulation of conventional (19) and ST (9, 20) EPR spectra for the case of isotropic motion and lends itself quite well to the consideration of restricted motion for both types of spectra, as shown by the results we report here.

Future work

Although the present simulations provide a useful illustration of the kinds of effects to be expected from changes in the amplitude of motion, a number of ap-

proximations prevent them from fitting experimental spectra accurately.

Our principal simplification, the use of axially symmetric magnetic tensors, makes the present simulations insensitive to rotation about the nitroxide principal axis. TEMPO (2,2,6,6-tetramethylpiperidine-1-oxyl) and doxyl spin labels have nearly axial hyperfine splittings but highly nonaxial g tensors (13), so this approximation only affects g effects on the spectra. The largest possible difference in the g_{YY} resonant field position is $(h\nu/g_{\perp}\beta-h\nu/g_{\parallel}\beta)/2$, which is approximately 4 G at X-band. This is much smaller than the 28-G shift due to hyperfine anisotropy, so the approximation is good for the wings but not for the central region of the spectrum. Our use of the adiabatic approximation for pseudosecular terms in the Hamiltonian (9, 19) also decreases the reliability of the central region of ST-EPR spectra (9). As a result, although the simulations are a good approximation to experimental results in the low- and high-field region, the simulations only indicate trends in the sensitivity of the central region. Direct use of the C''/C parameter plots will be less reliable than using empirical calibration plots to determine effective correlation times (8) and then using a plot like that in Fig. 9 to analyze the data, as illustrated above.

We are extending the present calculations to include nonaxial tensors and two-dimensional rotational diffusion. These calculations will make the central region of the spectrum much more accurate. Furthermore, for the transition rate method used in the present study, the adiabatic approximation can be removed by using methodology given by Sillescu and Kivelson (52) or Lange et al. (24). We have carried out this extension of the present method for V_1 spectra at $\tau_r = 10^{-7}$ s; the resulting spectra are in good agreement with those from the eigenfunction expansion method (29) for isotropic rotation.

We have kept the relaxation times T_1 and T_2 constant in our calculations, whereas for experimental systems these parameters should be determined for each individual case. These parameters are known to have an effect on the calculated ST-EPR spectra for isotropic motion (9) and would have similar effects on the spectra resulting from anisotropic motion.

These proposed refinements should make the calculations precise enough for accurate fitting of experimental spectra to simulations, as has been achieved for conventional EPR of oriented systems (53). However, even with these refinements, it is likely that changes in rate and amplitude will be difficult to distinguish unambiguously in the case of randomly oriented samples. Thus, experimental approaches to remove this ambiguity will probably be at least as important as refined calculations. This can be accomplished by using oriented samples to get the amplitude information directly (14, 34, 54) or performing time-resolved ST-EPR studies to measure rates directly (4, 7, 55, 56). Once one of these motion parameters is known, a plot such as that in Fig. 9 can be

used to determine the other. An alternative approach is to perform ST-EPR experiments at different spectrometer frequencies (57, 58) and obtain consistent rate and amplitude information that fit all spectra.

REFERENCES

1. Hemminga, M. A., and P. A. de Jager. 1989. Saturation transfer of spin labels: techniques and interpretation of spectra. *In* Biological Magnetic Resonance. Vol. 8. Spin Labeling Theory and Applications. L. J. Berliner and J. Reuben, editors. Plenum, New York. 131–178.

2. Hyde, J. S., and D. D. Thomas. 1980. Saturation-transfer spectroscopy. *Annu. Rev. Phys. Chem.* 31:293–317.

3. Marsh, D. 1989. Experimental methods in spin-label spectral analysis. *In* Biological Magnetic Resonance. Vol. 8. Spin Labeling Theory and Applications. L. J. Berliner and J. Reuben, editors. Plenum Press, New York. 255–337.

4. Robinson, B., H. Thomann, A. Beth, P. Fajer, and L. Dalton. 1985. The phenomenon of magnetic resonance: theoretical considerations. *In* EPR and Advanced EPR Studies of Biological Systems. L. R. Dalton, editor. CRC Press, Boca Raton, FL. 11–110.

5. Thomas, D. D. 1978. Large-scale rotational motions of proteins detected by electron paramagnetic resonance and fluorescence. *Biophys. J.* 24:439–462.

6. Thomas, D. D. 1985. Saturation transfer EPR studies of microsecond rotational motions in biological membranes. *In* The Enzymes of Biological Membranes. Vol. 1. A. Martonosi, editor. Plenum, New York. 287–312.

7. Thomas, D. D. 1986. Rotational diffusion of membrane proteins. *In* Techniques for the Analysis of Membrane Proteins. C. I. Ragan and R. J. Cherry, editors. Chapman & Hall, London. 377–431.

8. Squier, T. C., and D. D. Thomas. 1986. Methodology for increased precision in saturation transfer electron paramagnetic resonance studies of rotational dynamics. *Biophys. J.* 49:921–935.

9. Thomas, D. D., L. R. Dalton, and J. S. Hyde. 1976. Rotational diffusion studied by passage saturation transfer electron paramagnetic resonance. *J. Chem. Phys.* 65:3006–3024.

10. Huxley, A. F., and R. M. Simmons. 1971. Proposed mechanism of force generation in striated muscle. *Nature (Lond.).* 233:533–538.

11. Huxley, H. E. 1969. The mechanism of muscle contraction. *Science (Wash. DC).* 164:1356–1366.

12. Gaffney, B. J. 1979. Spin label-thiourea adducts. A model for saturation transfer EPR studies of slow anisotropic rotation. *J. Phys. Chem.* 83:3345–3349.

13. Griffith, O. H., and P. C. Jost. 1976. Lipid spin labels in biological membranes. *In* Spin Labeling: Theory and Applications. L. J. Berliner, editor. Academic, New York. 453–523.

14. Thomas, D. D., and R. Cooke. 1980. Orientation of spin-labeled myosin heads in glycerinated muscle fibers. *Biophys. J.* 32:891–906.

15. Mason, R. P., C. F. Polnaszek, and J. H. Freed. 1974. Comments on the interpretation of electron spin resonance spectra of spin labels undergoing very anisotropic rotational reorientation. *J. Phys. Chem.* 78:1324–1329.

16. Cannon, B., C. F. Polnaszek, K. W. Butler, L. E. G. Eriksson, and I. C. P. Smith. 1975. The fluidity and organization of mitochondrial membrane lipids of the brown adipose tissue of cold-adapted rats and hamsters as determined by nitroxide spin probes. *Arch. Biochem. Biophys.* 167:505–516.

17. Schreier, S., C. F. Polnaszek, and I. C. P. Smith. 1978. Spin labels in membranes. Problems in practice. *Biochim. Biophys. Acta.* 515:395–436.

18. McConnell, H. M. 1958. Reaction rates by nuclear magnetic resonance. *J. Chem. Phys.* 28:430–431.

19. McCalley, R. C., E. J. Shimshick, and H. M. McConnell. 1972. The effect of slow rotational motion on paramagnetic resonance spectra. *Chem. Phys. Lett.* 13:115–119.

20. Thomas, D. D., and H. M. McConnell. 1974. Calculation of paramagnetic resonance spectra sensitive to very slow rotational motion. *Chem. Phys. Lett.* 25:470–475.

21. Robinson, B. H., and L. R. Dalton. 1979. EPR and saturation transfer EPR at high microwave field intensities. *Chem. Phys.* 36:207–237.

22. Robinson, B. H., and L. R. Dalton. 1980. Anisotropic rotational diffusion studied by passage saturation transfer electron paramagnetic resonance. *J. Chem. Phys.* 72:1312–1324.

23. Robinson, B. H., and L. R. Dalton. 1981. Approximate methods for the fast computation of EPR and ST-EPR spectra. V. Application of the perturbation approach to the problem of anisotropic motion. *Chem. Phys.* 54:253–259.

24. Lange, A., D. Marsh, K.-H. Wassmer, P. Meier, and G. Kothe. 1985. Electron spin resonance study of phospholipid membranes employing a comprehensive line-shape model. *Biochemistry.* 24:4383–4392.

25. Kinosita, K., Jr., S. Kawato, and A. Ikegami. 1977. A theory of fluorescence polarization decay in membranes. *Biophys. J.* 20:289–305.

26. Kinosita, K., Jr., S. Kawato, and A. Ikegami. 1984. Dynamic structure of biological and model membranes: analysis by optical anisotropy decay measurement. *Adv. Biophys.* 17:147–203.

27. Lipari, G., and A. Szabo. 1980. Effect of librational motion on fluorescence depolarization and nuclear magnetic resonance relaxation in macromolecules and membranes. *Biophys. J.* 30:489–506.

28. Lipari, G., and A. Szabo. 1982. Model-free approach to the interpretation of nuclear magnetic resonance in macromolecules. 1. Theory and range of validity. *J. Am. Chem. Soc.* 104:4546–4559.

29. Freed, J. H., G. V. Bruno, and C. F. Polnaszek. 1971. Electron spin resonance lineshapes and saturation in the slow motional region. *J. Phys. Chem.* 75:3385–3399.

30. Horváth, L., and D. Marsh. 1983. Analysis of multicomponent saturation transfer ESR spectra using the integral method: application to membrane systems. *J. Magn. Reson.* 54:363–373.

31. Thomas, D. D., R. Cooke, and V. A. Barnett. 1983. Orientation and rotational mobility of spin-labelled myosin heads in insect flight muscle in rigor. *J. Muscle Res. Cell Motil.* 4:367–378.

32. Delmelle, M., K. W. Butler, and I. C. P. Smith. 1980. Saturation transfer electron spin resonance spectroscopy as a probe of anisotropic motion in model membrane systems. *Biochemistry.* 19:698–704.

33. Koole, P., C. Dijkema, G. Casteleijn, and M. A. Hemminga. 1981. A spin label saturation transfer ESR study of very slow anisotropic motion in oriented multibilayers of lecithin and cholesterol in the gel phase. *Chem. Phys. Lett.* 79:360–365.

34. Barnett, V. A., and D. D. Thomas. 1984. Saturation transfer electron paramagnetic resonance of spin-labeled muscle fibers: dependence of myosin head rotational motion on sarcomere length. *J. Mol. Biol.* 179:83–102.

35. Fajer, P. G., E. A. Fajer, N. J. Brunsvold, and D. D. Thomas. 1988. Effects of AMPPNP on the orientation and rotational dynamics of spin-labeled muscle cross-bridges. *Biophys. J.* 53:513–524.

36. Ludescher, R. D., and D. D. Thomas. 1988. Microsecond rotational dynamics of phosphorescent-labeled muscle cross-bridges. *Biochemistry.* 27:3343–3351.

37. Ostap, E. M., and D. D. Thomas. 1991. Rotational dynamics of spin-labeled F-actin during activation of myosin S1 ATPase using caged ATP. *Biophys. J.* 59:1235–1241.

38. Ostap, E. M., T. Yanagida, and D. D. Thomas. 1992. Orientational distribution of spin-labeled actin oriented by flow. *Biophys. J.* 63:966–975.

39. Thomas, D. D., S. Ishiwata, J. C. Seidel, and J. Gergely. 1980. Submillisecond rotational dynamics of spin-labeled myosin heads in myofibrils. *Biophys. J.* 32:873–890.

40. Hidalgo, C., D. D. Thomas, and N. Ikemoto. 1978. Effect of the lipid environment on protein motion and enzymatic activity of the sarcoplasmic reticulum calcium ATPase. *J. Biol. Chem.* 253:6879–6887.

41. Vriend, G., J. G. Schilthuis, B. J. M. Verduin, and M. A. Hemminga. Saturation-transfer ESR spectroscopy on maleimide spin-labeled cowpea chlorotic mottle virus. 1984. *J. Magn. Reson.* 58:421–427.

42. Fajer, P., and D. Marsh. 1983. Sensitivity of saturation transfer ESR spectra to anisotropic rotation. Application to membrane systems. *J. Magn. Reson.* 51:446–459.

43. Marsh, D. 1980. Molecular motion in phospholipid bilayers in the gel phase: long axis rotation. *Biochemistry.* 19:1632–1637.

44. Lapper, R. D., S. J. Paterson, and I. C. P. Smith. 1972. A spin label study of the influence of cholesterol in egg lecithin multibilayers. *Can. J. Biochem.* 50:969–981.

45. Thomas, D. D., D. J. Bigelow, T. C. Squier, and C. Hidalgo. 1982. Rotational dynamics of protein and boundary lipid in sarcoplasmic reticulum membrane. *Biophys. J.* 37:217–235.

46. Weber, G. 1977. Theory of differential phase fluorimetry: detection of anisotropic molecular motion. *J. Chem. Phys.* 66:4081.

47. Szabo, A. 1984. Theory of fluorescence depolarization in macromolecules and membranes. *J. Chem. Phys.* 81:150–167.

48. Wang, C. C., and R. Pecora. 1980. Time-correlation functions for restricted rotational diffusion. *J. Chem. Phys.* 72:5333–5340.

49. Meierovitch, E., A. Nayeem, and J. H. Freed. 1984. Analysis of protein-lipid interactions based on model simulations of electron spin resonance spectra. *J. Phys. Chem.* 88:3454–3465.

50. Polnaszek, C. F., G. V. Bruno, and J. H. Freed. 1973. ESR lineshapes in the slow-motional region: anisotropic liquids. *J. Chem. Phys.* 58:3185–3199.

51. Robinson, B. H., L. J. Slutsky, and F. P. Auteri. 1992. Direct simulation of continuous wave electron paramagnetic resonance spectra from Brownian dynamics trajectories. *J. Chem. Phys.* 96:2609–2616.

52. Sillescu, H., and D. Kivelson. 1968. Theory of spin-lattice relaxation in classical liquids. *J. Chem. Phys.* 48:3493–3505.

53. Fajer, P. G., R. L. H. Bennett, C. F. Polnaszek, E. A. Fajer, and D. D. Thomas. 1990. General method for multiparameter fitting of high-resolution EPR spectra using a simplex algorithm. *J. Magn. Reson.* 88:111–125.

54. Tanaka, H., and J. H. Freed. 1985. Electron spin resonance studies of lipid-gramicidin interactions utilizing oriented multibilayers. *J. Phys. Chem.* 89:350–360.

55. Fajer, P., D. D. Thomas, J. B. Feix, and J. S. Hyde. 1986. Measurement of rotational molecular motion by time-resolved saturation transfer electron paramagnetic resonance. *Biophys. J.* 50:1195–1202.

56. Schwartz, L. J., G. L. Millhauser, and J. H. Freed. 1986. Two-dimensional electron spin echoes: magnetization transfer and molecular dynamics. *Chem. Phys. Lett.* 127:60–67.

57. Johnson, M. E., and J. S. Hyde. 1981. 35-GHz (Q-band) saturation transfer electron paramagnetic resonance studies of rotational diffusion. *Biochemistry.* 20:2875–2880.

58. Johnson, M. E., L. Lee, and L. W.-M. Fung. 1982. Models for slow anisotropic rotational diffusion in saturation transfer electron paramagnetic resonance at 9 and 35 GHz. *Biochemistry.* 21:4459–4467.

59. Polnaszek, C. F., D. Marsh, and I. C. P. Smith. 1981. Simulation of the EPR spectra of the cholestane spin probe under conditions of slow axial rotation. Application to gel phase dipalmitoyl phosphatidyl choline. *J. Magn. Reson.* 43:54–64.

60. Beth, A. H., R. Wilder, L. S. Wilkerson, R. C. Perkins, B. P. Meriwether, L. R. Dalton, C. R. Park, and J. H. Park. 1979. EPR and saturation transfer EPR studies on glyceraldehyde 3-phosphate dehydrogenase. *J. Chem. Phys.* 71:2074–2082.

61. Hemminga, M. A., and A. J. Faber. 1986. Analysis of anisotropic spin-label motion in saturation-transfer ESR spectra of spin-labeled cowpea chlorotic mottle virus. *J. Magn. Reson.* 66:1–8.

62. Jost, P., L. Libertini, V. C. Hebert, and O. H. Griffith. 1971. Lipid spin labels in lecithin multilayers. A study of motion along fatty acid chains. *J. Mol. Biol.* 59:77–98.